Purdue University

Purdue e-Pubs

International Refrigeration and Air Conditioning Conference

School of Mechanical Engineering

2022

Experimental Study Of Falling Film Evaporation Of R1234ze(E) And R134a In An Innovative Shell-And-Tube Heat Exchanger

Giuseppe Censi

Andrea Padovan

Follow this and additional works at: https://docs.lib.purdue.edu/iracc

Censi, Giuseppe and Padovan, Andrea, "Experimental Study Of Falling Film Evaporation Of R1234ze(E) And R134a In An Innovative Shell-And-Tube Heat Exchanger" (2022). *International Refrigeration and Air Conditioning Conference.* Paper 2406.
https://docs.lib.purdue.edu/iracc/2406

This document has been made available through Purdue e-Pubs, a service of the Purdue University Libraries. Please contact epubs@purdue.edu for additional information.
Complete proceedings may be acquired in print and on CD-ROM directly from the Ray W. Herrick Laboratories at https://engineering.purdue.edu/Herrick/Events/orderlit.html

Experimental Study Of Falling Film Evaporation Of R1234ze(E) And R134a In An Innovative Shell-And-Tube Heat Exchanger

Giuseppe CENSI*, Andrea PADOVAN

Onda S.p.A.,
Lonigo, VI, Italy
Phone: +39 0444720720, Fax: +39 0444720721,
E-mail: gcensi@onda-it.com, apadovan@onda-it.com

* Corresponding Author

ABSTRACT

Falling film evaporators are an efficient alternative to flooded evaporators: like them, they allow to reach low water-to-saturation temperature approaches, but they significantly limit the amount of refrigerant. This work presents results obtained with an innovative concept of falling film shell-and-tube evaporator, where a liquid film of refrigerant falls down from top to bottom, redistributing itself on each row of tubes by means of special perforated plates. The study presents the experimental heat transfer performance of a prototype, comparing it to that of an equivalent flooded evaporator, in the same chiller, using 19.05 mm OD copper tubes with increased surface. The tests are performed with constant outlet water temperature (7 °C) and constant water flowrate. The average heat flux varies between 15 and 35 kW m^{-2}, and the water-to-saturation approach between 1 and 2 K. The water to be chilled enters at the bottom part of the heat exchanger, and flows in four passages, at the beginning and at the end of each of them the temperature is measured. The measure of heat flow rate on each water passage allows to estimate how the heat flux and the refrigerant side heat transfer coefficient are distributed inside the exchanger, both for R134a and for its widely accepted low-GWP alternative R1234ze(E). The achieved water-to-saturation temperature approach is similar to that relative to the flooded evaporator, and the refrigerant heat transfer coefficient of R1234ze(E) is lower than that of R134a. For both fluids, it appears to be lower where the heat flux is greater. The heat transfer coefficient calculated by means of a model inspired to that proposed by Christians and Thome (2012b) showed a good agreement with the experimental results.

1. INTRODUCTION

Greenhouse gas emission due to human activity is a major cause of the climate change, and refrigeration and air conditioning play an important role: the past generation refrigerant fluids (hydrofluorocarbons, HFC) must be progressively phased out since they in general present an unacceptable global warming potential (GWP). Currently HFCs are increasingly replaced by pure hydrofluoro-olefins (HFOs), or blends HFC/HFO, sometimes including hydrocarbons (HC).

In particular, the present work deals with the substitution of the pure HFC fluid R134a with the pure HFO fluid R1234ze(E), a choice already largely dominant in the Europe market, which begins to consolidate even in the US one. As compared to R134a, whose global warming potential over 100 years (GWP_{100}) is equal to 1300 (Hodnebrog et al., 2013), the GWP_{100} of R1234ze(E) is less than 1. On the other side, R1234ze(E) is slightly flammable and its volumetric capacity is 25 % lower than the one of R134a. A comprehensive detailed theoretical study on thermodynamic efficiency and the role of the thermo-physical properties of R1234ze(E) and R513A (together with other low GWP fluids) can be found in McLinden et al. (2017).

With an impact depending on the fluctuations of the price in the market, a limitation of the amount of the charge of refrigerants in vapor compression cycles (VCC) is always welcome. This is true especially for R1234ze(E), whose safety classification implies additional certification costs related to its charge. On this regard, for centrifugal systems it is almost mandatory to find heat exchangers alternative to flooded evaporators, which typically require a big

amount of refrigerant. Due to the good efficiency guaranteed by flooded evaporators, the challenge is to design new evaporators with lower refrigerant charge but same performance. An increasingly adopted option consists of horizontal falling film or spray evaporators, whose tubes, instead to be flooded in a common pool, are wet one-by-one by a thin film of liquid. Basically, heat is transferred by conduction and convection across the liquid film, with phase change occurring at the liquid-vapour interface, and nucleate boiling in the liquid film.

As regards a direct comparison of R134a and R1234ze(E) during pool boiling on enhanced surfaces, one of the first studies is due to Van Rooyen and Thome (2013). They evaluated the pool boiling performances of R134a, R236fa, and R1234ze(E) in two enhanced tubes, both with a structured surface. At saturation temperatures of 5 and 25 °C, and with heat fluxes of 15 to 70 kW m^{-2}, the heat transfer coefficients of R1234ze(E) and R134a were measured very similar. Among the recent works, Gorgy (2016) measured the pool boiling heat transfer coefficient of R134a, R1234ze(E), R450A, R123, and R1233zd(E), in a highly enhanced tube. At the saturation temperature of 4.44 °C, and in the heat flux range 10-110 kW m^{-2}, within the uncertainty of measurement the performances of R1234ze(E) and R134a were found almost equal. Byun et al. (2017), on the other hand, found some differences between the two fluids. They compared the pool boiling heat transfer performances of R134a, R1234ze(E), and R1233zd(E), in a plain tube and in two different enhanced tubes with structured surfaces. For all the tubes, and for two different evaporation temperatures (4.4 °C and 26.7 °C), with heat fluxes between from 10 to 50 kW m^{-2}, the heat transfer coefficient of R1234ze(E) was found lower than that of R134a of an amount variable between 10 and 20 %.

With respect to a comparison between the performances of the falling film evaporation and pool boiling, in the open literature the fluid R134a is widely studied, whereas no work regarding R1234ze(E) is at present authors' knowledge. Roques and Thome (2007) tested R134a, and Christians and Thome (2012a) tested R134a and R236fa, during pool boiling and falling film on structured surfaces at a saturated temperature of 5 °C and heat fluxes of less than 100 kW m^{-2}. Their results show, for falling film evaporation, higher heat transfer coefficients than for pool boiling, in a measure depending on the characteristics of the surface: in some cases, the performances tend to approach at high heat fluxes. Different results were found by Ji et al. (2019), who studied R134a during pool boiling and falling film, at 11 °C from 10 to 50 kW m^{-2}. The test tubes, enhanced with a structured surface, achieved better results in falling film evaporation when the heat flux was less than 30 kW m^{-2}, whereas they started to worsen compared to pool boiling at higher heat fluxes.

Despite the advantages, considering a whole bundle of tubes, the spray or falling film evaporators present some complications with respect to flooded evaporators. They require a complex distribution system for the liquid inlet and for the dissipation of the flash gas, and particular care in the alignment of the tubes, in order to guarantee uniformity in the liquid supply and avoid dry patches on the tubes wall. Furthermore, dryout can occur at the lowest tube rows of the bundle, especially when the flowrate is reduced, for example at partial loads. Depending on geometry, operating conditions and fluid properties, it is possible to identify up to five different flow patterns, and, among them, mainly three are distinguished: sheet, jet (column), and droplet modes. In particular, the first seems to develop the highest heat transfer coefficient, but there is not clear agreement about the causes between different researchers (Fernández-Seara and Pardiñas, 2014). Anyway, it is confirmed that the two-phase flow pattern plays a role in the thermal modelling, with specific correlations as a function of the flow regime (for example, Zhao et al. 2016).

Another critical issue to be properly considered is the vapour flow. In classical falling film evaporators, a big volume of the shell is usually required to avoid liquid entrainment to the compressor. Besides, the ascending vapour can modify the trajectory of the falling liquid, affecting the heat transfer performance, as investigated for example by Ji et al. (2016). Detailed reviews of the studies focused on the design and the effects of the distribution systems and tube layouts, and on the influence of flow pattern and vapour flow, can be found in Ribatski and Jacobi (2005), Abed et al. (2014), Fernández-Seara and Pardiñas (2014).

The evaporator tested in the present work mixes falling film and pool boiling processes on each row of tubes. Special plates retain part of the liquid falling down, slowing it down and supposedly improving the distribution on every row. Censi et al. (2018, 2019) conducted an experimental study in such an evaporator prototype, with R134a and R1234ze(E) at 6 °C from 15 to 35 kW m^{-2}, finding refrigerant heat transfer coefficients similar to those of the flooded evaporator. When used in a vapor compression cycle, this evaporator allows to reach a coefficient of performance (COP) 10 % higher than that of a direct expansion evaporator, like the flooded type, but without a significant increase in the refrigerant charge. In the present work, the investigation of the performances is pushed deeper on the analysis of the refrigerant heat transfer coefficient.

2.EXPERIMENTAL PROTOTYPE

2.1 Operating description

The heat exchanger considered in this work is described in Figure 1: it is essentially a falling film evaporator, with in addition special devices designed to improve the refrigerant distribution.

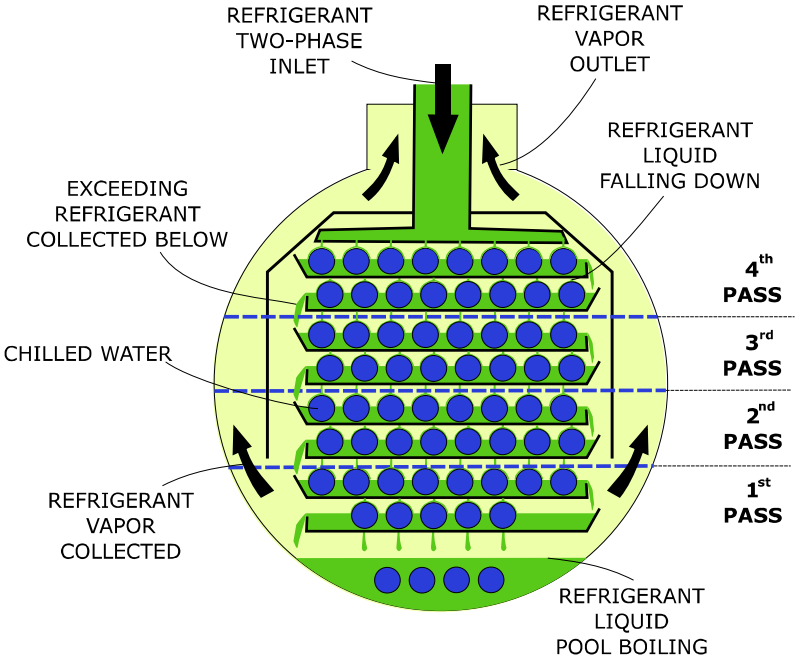

Figure 1: Schematic view of the falling film evaporator tested. The water enters at the bottom and flows in four passages, as indicated by the dashed lines.

This falling film evaporator is though to keep the refrigerant charge as low as possible and to achieve, or to improve, the performances of the flooded evaporator. Besides, it aims to avoid some of the classical problems of falling film: the difficult distribution, the dryout occurring at non-nominal conditions, and the large dimensions, all discussed in the Introduction. The resulting final design is illustrated in Figure 1, and the detailed operating principles are reported by Censi et al. (2018, 2019). Unlike the classical film evaporators, this evaporator includes special perforated plates with vertical longitudinal borders placed below each tube row. The plates aim to solve two different problems connected to the falling film evaporation. First, they help to supply liquid to the lower tubes and to minimize or avoid dryout phenomena: thus, they should work as "liquid catchers", similarly to the devices described by Chang and Chiou (1999). Additionally, they should prevent liquid maldistribution, both along the width direction and the length direction, whose effects are studied and illustrated, for example, by Yang and Wang (2011).

It is worth noting that, due to the plate drilling, the liquid flow pattern from the upper plate to the lower row of tubes can be classified mainly as column mode. This flow regime was confirmed by visualizations carried out in a separate prototype with water in adiabatic single-phase flow.

Table 1: Characteristics of the falling film evaporator prototype.

Parameter	**Value**	**Parameter**	**Value**
Tube name	Gewa-B6H	Tube length	1016 mm
Tube surface	Structured	N. of tube passes	4
Tube outside diameter	19.05 mm	Shell outside diameter	610 mm

2.2 Characteristics of the prototype

The tubes used have structured external surface, specifically designed for pool boiling. The surface is enhanced by fins with a dedicated shape, in order to create sites that promote nucleate boiling at low temperature differences, of the type, for example, presented by Bergles (1997). Under moderate heat fluxes, they are the best choice for flooded evaporators.

As regards falling film, instead, no specific enhanced tubes exist. Anyway, the structured surfaces seem the most suitable, as, in general, they let the liquid flow longitudinally and promote the sheet flow mode. The evaporator design, which works under column flow mode but with a pool boiling part, present in almost each row of tubes, suggests using structured surface. In particular, the tube model of the present prototype is Gewa-B6H, provided by Wieland, with outside nominal diameter 19.05 mm. Possible future studies will show if other surfaces, for example low-finned, are suitable for the hybrid film.

The geometry of the prototype is summarized in Table 1.

3.EXPERIMENTAL STUDY

3.1 Experimental apparatus

The experimental tests were run on the test facility set up at the laboratory of Onda S.p.A., Italy, schematic of which is depicted in Figure 2. It represents a classical vapor compression system (compressor, condenser, expansion device, evaporator), with an additional subcooler downstream of the condenser. The compressor is centrifugal and oil free, with axial and radial magnetic bearings. For the tests, the system was charged with R134a first, and then with R1234ze(E); between the two operations, the plant was cleaned with nitrogen and the electronic regulation system of the compressor was re-set.

The superheated vapour at high pressure flows from the compressor to the shell-and-tube condenser, where it is fully condensed and then further subcooled in a brazed-plate heat exchanger. The subcooling level can be independently controlled, varying the cooling water temperature and flow rate. As a result, it is possible to achieve the set vapour quality at the inlet of the test evaporator.

The expansion device is a step motor electronic valve, whose opening is varied manually according to the required liquid level at the evaporator, maintained constant. After reducing pressure through the expansion valve, the refrigerant flows to the evaporator and finally to the compressor, again. A sight glass is placed between the evaporator and the compressor to check that there is not entrainment of liquid drops in the vapour flow. Furthermore, the isentropic efficiency of the compressor is measured and compared to that declared by the compressor manufacturer.

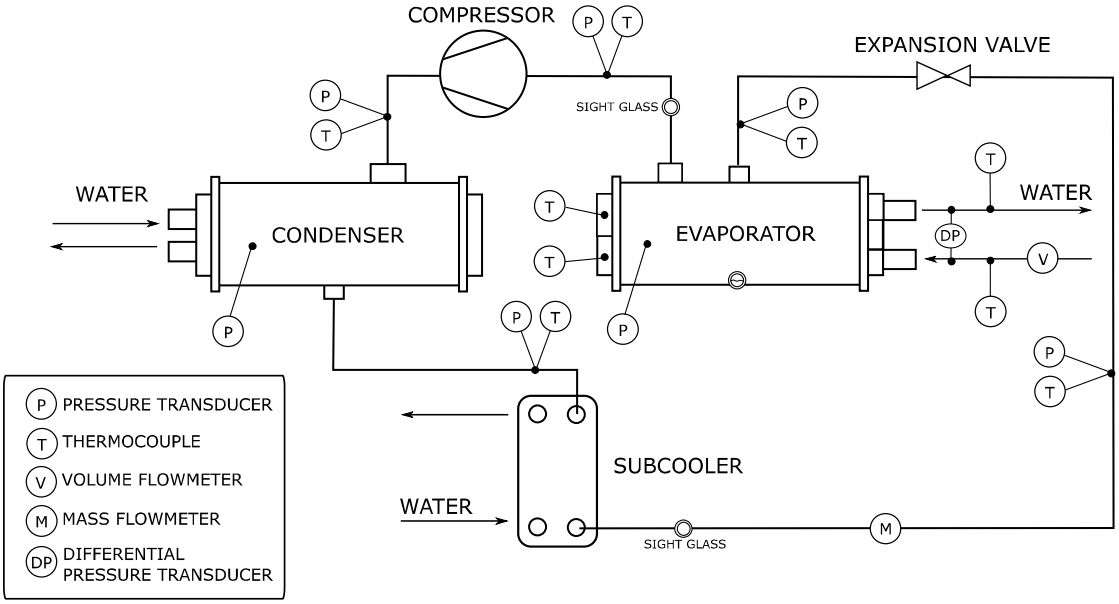

Figure 2: Schematic drawing of the experimental test rig.

Water is used as secondary fluid to vaporize R134a and R1234ze(E). The water temperature at the inlet and outlet of each passage on the test evaporator is measured by thermocouples inserted in adiabatic sections, where perfect mixing is assured. Type J thermocouples connected to a Kaye ice point instrument as zero reference system are used. Thermocouples were calibrated on site using a primary Pt100 probe and a reference bath to get the accuracy value reported in Table 1. The water volume flow rate and pressure drop through the evaporator are measured with an electromagnetic flow meter and a differential pressure transducer, respectively. Thermocouples and pressure transducers are also installed in different sections of the refrigerant loop to get all the measurements needed for the data reduction. The saturation temperature at the evaporator is obtained by the pressure, which is taken both inside the shell and at the evaporator outlet. A Coriolis effect flow meter measures directly the refrigerant mass flow rate. In this way, the thermal balances on both water and refrigerant side are compared and checked. The mean deviation is found to be around 3%. The accuracies for sensors and parameters (described in the next section) are listed in Table 2; the estimation is done according to the method by Kline and McClintock (1953).

3.2 Data reduction and operative conditions

In order to understand the behavior at different loads, the compressor capacity was varied by means of an inverter, maintaining constant the evaporator inlet vapor quality at 0.18 kg kg^{-1}.

The average heat flux for each passage, and for the whole evaporator, is given by the water side heat flow rate divided by the reference area, that is the external envelope plain tube surface area at the nominal diameter. The average value ranges from 19 to 33 kW m^{-2}, while the heat flux on each water passage varies from 9 to 65 kW m^{-2}.

The global heat transfer coefficient, considered at the shell, is then calculated for each passage and for the whole evaporator, dividing the heat flux by the water-to-saturation mean temperature difference. The saturation temperature comes from the pressure measured inside the shell. The external heat transfer coefficients are obtained by a thermal resistance subtraction: the tube-side heat transfer coefficient is calculated by means of an empirical based correlation provided by the tube manufacturer and verified by means of ad hoc single-phase tube-in-tube experimental tests. The present procedure is affected by uncertainty, up to almost 20 % (Table 2).

All the thermo-physical properties of R134a, R1234ze(E) and water are calculated by means of the Refprop 10.0 software (Lemmon et al., 2018).

Table 2: Accuracy for sensors and parameters (at typical test conditions), estimated according to the method by Kline and McClintock (1953).

Parameter	**Accuracy**	**Parameter**	**Accuracy**
Temperature	±0.07 K	Temp. difference	±0.10 K
Volumetric flow rate	±0.5 %	Heat flux	±3 %
Mass flow rate	±0.5 %	Global heat transf. coeff.	±5 %
Absolute pressure	±1 kPa	Mean refrigerant heat trans. coeff.	±18 %

3.3 Experimental results

This section describes the experimental results of global and refrigerant heat transfer coefficient; the evaporator water leaving temperature is 7 °C, the inlet vapor quality at the evaporator is 0.18 and the refrigerant saturation temperature is 5.5 °C (±0.5 K). The graph in Figure 3 reports the heat flux in the tubes of the first and third pass of the falling film evaporator as a function of the liquid film Reynolds number:

$$Re_f = 2\, m_{ref,l}/(L_t\, \mu_{ref,l}) \quad (1)$$

The experimental uncertainty band of the heat flux is reported for each point. Both the heat flux and the film Reynolds number are the mean values measured in the tubes of each pass. The tubes of the first pass are in the bottom part of the evaporator whereas the tubes of the third pass are in the upper part of the evaporator. The liquid film Reynolds number decreases when passing from the third to the first pass because some amount of liquid evaporates when the refrigerant falls through each row of tubes. On the other hand, the heat flux of the tubes in the first pass is significantly higher than that of the tubes in the third pass because the water enters at first the tubes of the first pass at higher temperature and then is cooled in each passage; this results in a higher water to saturation

temperature difference and a higher heat flow rate exchanged in the first pass. For the same data reported in Figure 3, in the graph of Figure 4 the mean refrigerant heat transfer coefficient measured in the tubes of the first and third pass is plotted as a function of the liquid film Reynolds number. In the third pass the experimental uncertainty of heat transfer coefficient increases up to ±35% because the water to saturation temperature difference is small.

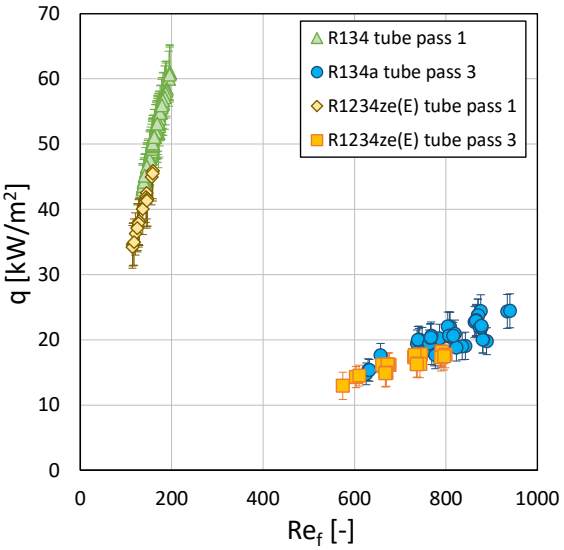

Figure 3: Experimental heat flux vs. liquid film Reynolds number in the tubes of the first and third pass of the falling film evaporator with R134a and R1234ze(E).

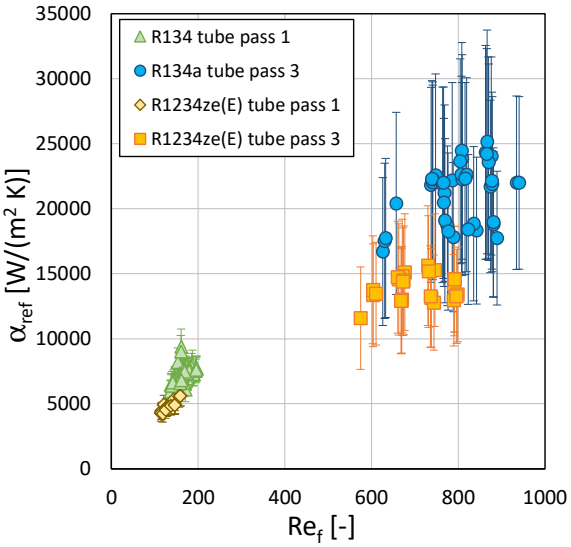

Figure 4: Experimental refrigerant (R134a and R1234ze(E)) heat transfer coefficient vs. liquid film Reynolds number in the tubes of the first and third pass of the falling film evaporator.

For both the fluids the heat transfer coefficient increases with increasing the liquid film Reynolds number. In these data the heat flux increases with increasing the liquid film Reynolds number, because in the present experimental apparatus, a vapor compression system, the heat flow rate and the refrigerant flow rate cannot be controlled independently. At the same value of film Reynolds number, the heat transfer coefficient of R1234ze(E) is always lower than that of R134a, despite the experimental uncertainty in the third pass data is high. Although the heat flux of the tubes of the first pass is higher than that of the tubes in the third pass, their heat transfer coefficient is lower; this confirms that the film Reynolds number, and so the feed of the tubes, affects the heat transfer. As reported in the literature (for instance Christians and Thome 2012a, 2012b), partial dry-out of the tubes occurs below a threshold value of film Reynolds number: the tubes are not more uniformly wet, dry patches appear on the wall and the heat transfer coefficient drops down.

In Figure 5 the global heat transfer coefficient of the falling film evaporator with refrigerants R134a and R1234ze(E) is plotted as a function of heat flux; the reported data have the same internal (water) heat transfer coefficient, 15 kW m^{-2} K^{-1}, thus differences in the heat transfer coefficient are exclusively due to the behavior of the refrigerant.

The water velocity inside the tubes is 1.2 m s^{-1}, which is a typical value for heat exchangers. With R134a the global heat transfer coefficient is around 7% higher than when operating with R1234ze(E). Figure 6 compares the experimental heat transfer coefficients of R134a and R1234ze(E) in the falling film evaporator. In the two graphs the heat transfer coefficients are the average values of all the tubes. The heat transfer coefficient of R1234ze(E) is on average 15% lower than that of R134a and differences up to around 20% can be observed for example at 25 kW m^{-2} heat flux.

In Figure 7 the global heat transfer coefficient of the falling film evaporator is compared to that of the flooded evaporator; the refrigerant is R134a and the internal (water) heat transfer coefficient is constant and equal to 15 kW m^{-2} K^{-1}. The global heat transfer coefficients of the two evaporators are similar.

In Figure 8 the R134a heat transfer coefficient data of the falling film and flooded evaporators are compared. On average, the falling film heat transfer coefficient is 10% lower than that of the flooded evaporator. The water side thermal resistance reduces the performance difference between the two evaporators.

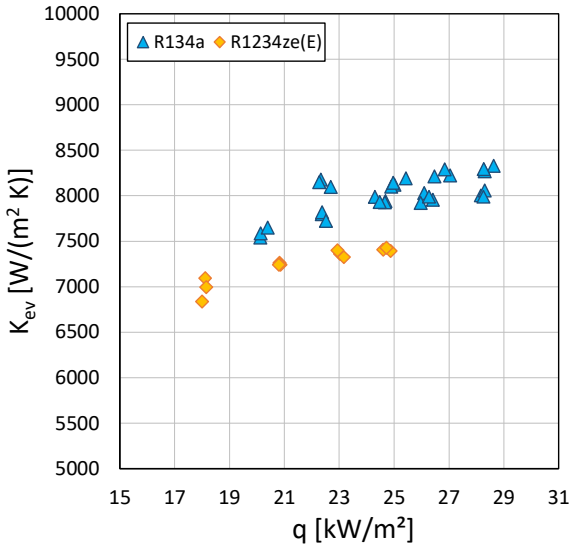

Figure 5: Experimental global heat transfer coefficient vs. heat flux for the falling film evaporator with R134a and R1234ze(E); the internal heat transfer coefficient is constant and equal to 15 kW m^{-2} K^{-1}.

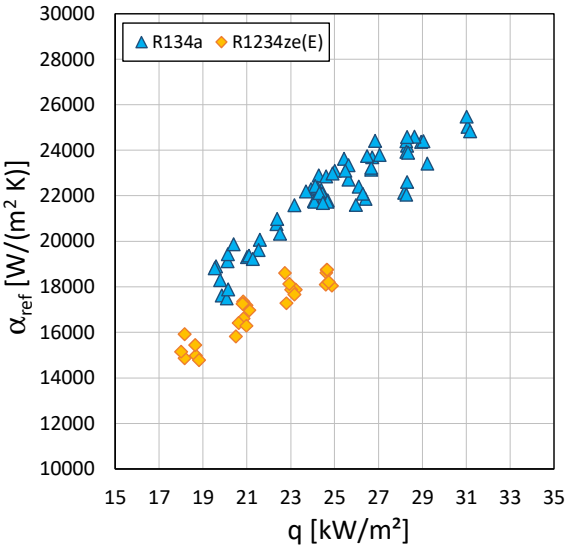

Figure 6: Experimental mean refrigerant (R134a and R1234ze(E)) heat transfer coefficient vs. heat flux for the falling film evaporator.

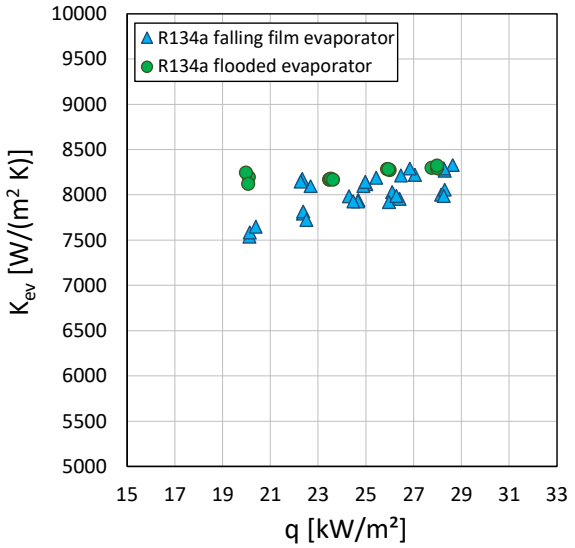

Figure 7: Experimental global heat transfer coefficient vs. heat flux for the falling film and flooded evaporator with R134a; the internal heat transfer coefficient is constant and equal to 15 kW m^{-2} K^{-1}.

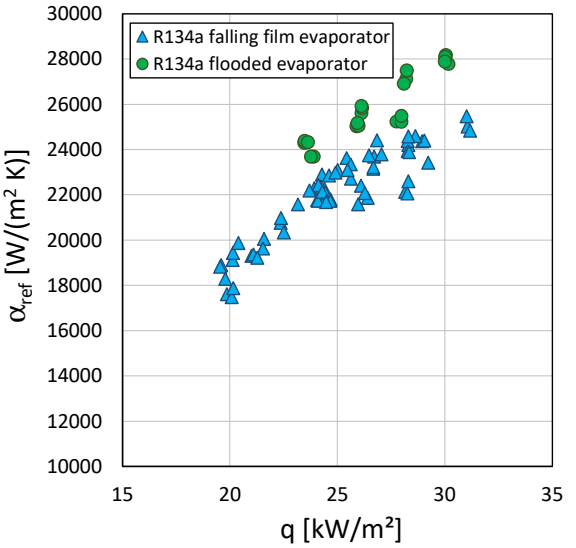

Figure 8: Experimental mean R134a heat transfer coefficient vs. heat flux for the falling film and flooded evaporator.

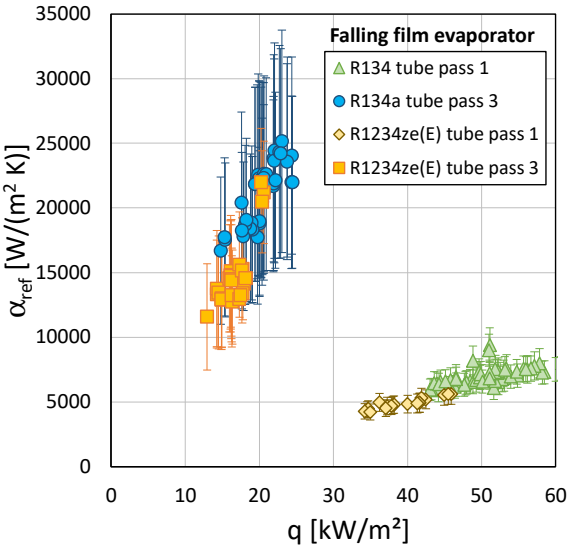

Figure 9: Experimental refrigerant (R134a and R1234ze(E)) heat transfer coefficient vs. heat flux in the tubes of the first and third pass of the falling film evaporator.

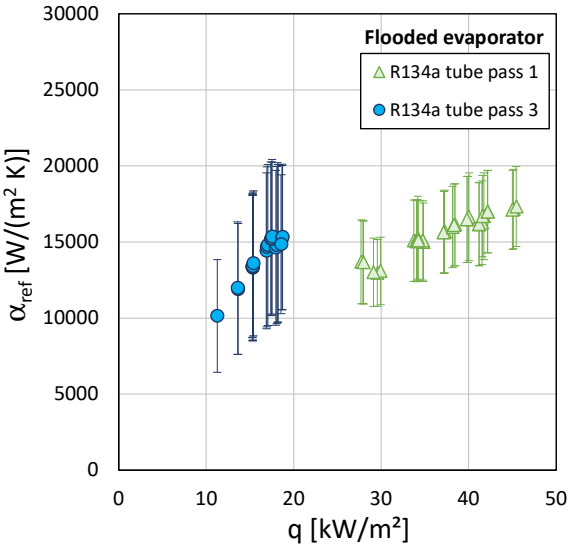

Figure 10: Experimental R134a heat transfer coefficient vs. heat flux in the tubes of the first and third pass of the flooded evaporator.

Figure 9 and Figure 10 report the experimental refrigerant heat transfer coefficient in the tubes of the first and third pass as a function of the heat flux for the falling film and the flooded evaporators. For each point the experimental uncertainty band of heat transfer coefficient is reported. For both the evaporators the tubes of the first pass, where the water enters, are in the bottom part of the evaporator. When comparing the R134a data of the two graphs, at the same values of heat flux, in the tubes of the third pass the falling film heat transfer coefficient is even higher than that of the flooded evaporator (data with heat flux between around 10 to 20 kW m^{-2}). On the contrary, when comparing the data of the tubes of the first pass, at the same value of heat flux the heat transfer coefficient of the flooded evaporator is nearly three times higher than that of the falling film evaporator (data with heat flux between around 30 to 50 kW m^{-2}).

4. MODELING OF FALLING FILM HEAT TRANSFER COEFFICIENT

The mean values of refrigerant heat transfer coefficient measured in the falling film evaporator have been compared with the calculated values given by an empirical prediction correlation. The correlation has the same form as proposed by Christians and Thome (2012b), where new coefficients have been calculated based on the fitting of the present experimental data of mean heat transfer coefficients:

$$\alpha_{ref,cal} = a\,[(q^2\,D_t)/(h_{lv}^{5/2}\,\mu_{ref,l}\,/(\rho_{ref,l}-\rho_{ref,v}))]^b\,G_{t\text{-}s}^{1.2449} \quad (2)$$

First, the parameter $G_{t\text{-}s}$, which accounts for the type of tube, has been optimized keeping the original value of coefficients a and b. Then, new values for the two coefficients have been obtained. The new coefficients values are: $G_{t\text{-}s}$ = 0.1285, a = 1979000 and b = 0.2734. As shown in Figure 11 the correlation predicts the present experimental data within ±20%.

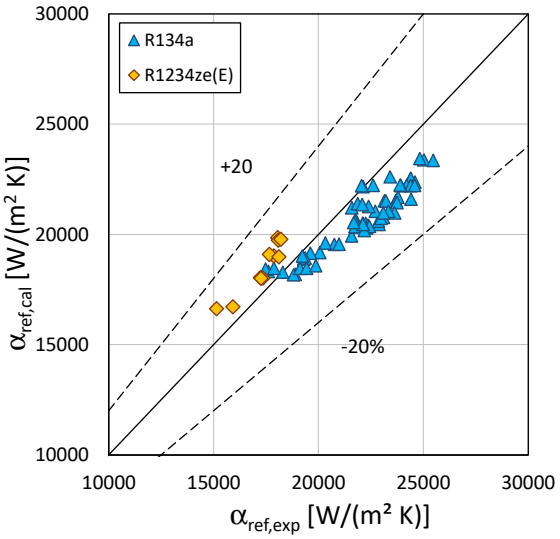

Figure 9: Calculated vs. experimental falling film heat transfer coefficient (R134a and R1234ze(E)).

5. CONCLUSIONS

The present paper describes an experimental investigation on a falling film evaporator working with refrigerants R134a and R1234ze(E). In the first part of the experimental study, the R134a and R1234ze(E) heat transfer coefficients are compared and discussed. In the second part, the R134a heat transfer coefficients measured in the falling film evaporator are compared with those measured in a flooded evaporator with similar number and layout of tubes. Finally, a preliminary modeling of the falling film evaporator heat transfer coefficient is proposed.
The results show that:

- the R134a falling film heat transfer coefficient is higher than that of R1234ze(E);
- the refrigerant heat transfer coefficient of the falling film evaporator is strongly affected by the position of the tubes row: although their heat flux is significantly higher, the tubes in bottom rows of the evaporator (first pass), which are characterized by the lower values of film Reynolds number, exhibit a significantly lower heat transfer coefficient as compared to the tube of the upper rows (third pass);
- at the same heat flux the heat transfer coefficients of the bottom rows of tubes (first pass) of the flooded evaporator are three times higher than those measured in the falling film evaporator; on the contrary, in the tubes of the third pass the falling film heat transfer coefficient is even higher than that of the flooded evaporator;
- A correlation with the same structure as by Christians and Thome (2012b) has been used to predict the mean refrigerant heat transfer coefficient of the falling film evaporator: agreement within ±20% between calculated and experimental data is obtained.

NOMENCLATURE

D	diameter	(m)
h_{lv}	latent heat of vaporization	(J kg^{-1})
K	global heat transfer coefficient	(W m^{-2} K^{-1})
L	length	(m)
m	mass flow rate	(kg s^{-1})
q	heat flux	(W m^{-2})
Re	Reynolds number	(-)
α	heat transfer coefficient	(W m^{-2} K^{-1})
μ	dynamic viscosity	(Pa s)
ρ	density	(kg m^{-3})

Subscript

ev	evaporator
f	film
l	liquid
ref	refrigerant
t	tube
v	vapor

REFERENCES

Abed, M.A., Alghoul, M.A., Yazdi, M.H., & Al-Shamani, A.N., 2015. The role of enhancement techniques on heat and mass transfer characteristics of shell and tube spray evaporator: a detailed review. Appl. Therm. Eng. 77, 923-940.

Bergles, A.E., 1997. Heat Transfer Enhancement - The Maturing of Second-Generation Heat Transfer Technology. Heat Transfer Eng., 18(1), 47-55.

Byun, H.-W., Kim, D.H., Yoon, S.H., Song, C.H., Lee, K.H., & Kim, O.J., 2017. Pool boiling performance of enhanced tubes on low GWP refrigerants. Appl. Therm. Eng. 123, 791-798.

Censi, G., Giancotti, L., & Padovan, A., 2018. Experimental investigation of a new low-approach evaporator with reduced refrigerant charge. International Refrigeration and Air Conditioning Conference at Purdue, West Lafayette, Indiana, USA.

Censi, G., Giancotti, L., & Padovan, A., 2019. Experimental comparison of the heat transfer performance of R134a and R1234ze(E) in a hybrid film evaporator. Refrigeration Science and Technology1431, 2706–2713.

Chang, T.B., Chiou, J.S., 1999. Spray evaporation heat transfer of R-141b on a horizontal tube bundle. Int. J. Heat Mass Transf. 42, 1467–1478.

Christians, M., & Thome, J.R., 2012a. Falling film evaporation on enhanced tubes, part 1: Experimental results for pool boiling, onset-of-dryout and falling film evaporation. Int. J. Refrigeration 35, 300-312.

Christians, M., & Thome, J.R., 2012b. Falling film evaporation on enhanced tubes, part 2: Prediction methods and visualization. Int. J. Refrigeration 35, 313-324.

Fernández-Seara, J., & Pardiñas, Á. Á, 2014. Refrigerant falling film evaporation review: Description, fluid dynamics and heat transfer. Appl. Therm. Eng. 64(1), 155-171.

Gorgy, E., 2016. Nucleate boiling of low GWP refrigerants on highly enhanced tube surface. Int. J. Heat Mass Transf. 96, 660–666.

Hodnebrog, Ø., Etminan, M., Fuglestvedt, J.S., Marston, G., Myhre, G., Nielsen, C.J., Shine, K.P., & Wallington, T J., 2013. Global Warming Potentials and Radiative Efficiencies of Halocarbons and Related Compounds: A Comprehensive Review. Rev. Geophys. 51(2), 300-378.

Ji, W.-T., Zhao, C.-Y., Zhang, D.-C., Yoshioka, S., He, Y.-L., & Tao, W.-Q., 2016. Effect of vapor flow on the falling film evaporation of R134a outside a horizontal tube bundle. Int. J. Heat Mass Transf. 92, 1171-1181.

Ji, W.-T., Zhao, E.-T., Zhao, C.-Y., Zhang, H., & Tao, W.-Q., 2019. Falling film evaporation and nucleate pool boiling heat transfer of R134a on the same enhanced tube. Appl. Therm. Eng. 147, 113-121.

Kline, S.J., & McClintock, 1953. Describing the uncertainties in single-sample experiments. Mechanical Engineering, 75, 3-8.

Lemmon, E.W., Bell, I.H., Huber, M.L., & McLinden, M.O., 2018. NIST Standard Reference Database 23: Reference Fluid Thermodynamic and Transport Properties-REFPROP, Version 10.0. Standard Reference Data Program. Gaithersburg, USA.

McLinden, M.O., Brown, J.S., Brignoli, R., Kazakov, A.F., & Domanski, P.A., 2017. Limited options for low-global-warming-potential refrigerants. Nature Comm. 8: 14476.

Ribatski, G., & Jacobi, A.M., 2005. Falling-film evaporation on a horizontal tubes a critical review. Int. J. Refrigeration 28, 635-653.

Roques, J.F., & Thome, J.R., 2007. Falling Films on Arrays of Horizontal Tubes with R-134a, Part I: Boiling Heat Transfer Results for Four Types of Tubes. Heat Transfer Eng., 28(5), 394-414.

Van Rooyen, E., & Thome, J.R., 2013. Pool boiling data and prediction method for enhanced boiling tubes with R-134a, R-236fa, and R-1234ze(E). Int. J. Refrigeration 36 (2), 447-455.

Yang, L., & Wang, W., 2011. The heat transfer performance of horizontal tube bundles in large falling film evaporators. Int. J. Refrigeration, 34(1), 303-316.

Zhao, C.-Y., Ji, W.-T., Jin, P.-H., & Tao, W.-Q., 2016. Heat transfer correlation of the falling film evaporation on a single horizontal smooth tube, Appl. Therm. Eng. 103, 177-186.